J. Fluid Mech. (1989), *vol.* 201, *pp.* 13–34
Printed in Great Britain

Degeneracies of the temporal Orr–Sommerfeld eigenmodes in plane Poiseuille flow

By RAJARATNAM SHANTHINI
Division of Fluid Mechanics, Luleå University of Technology, S-951 87 Luleå, Sweden

(Received 21 April 1988)

Degenerating stable temporal Orr–Sommerfeld eigenmodes are studied for plane Poiseuille flow. The discrete spectrum of the eigenmodes is shown to possess infinitely many degeneracies, each appearing at a certain combination of k (the modulus of resultant wavenumber) and αR (the streamwise wavenumber time the Reynolds number). The eigenmodes are found to degenerate in a specific manner which confines the streamwise phase velocities of the degeneracies to be around $\frac{2}{3}$ of the centreline velocity. The responses of the degeneracies are investigated through the initial-value problem. The responses of the first four symmetric and the first two antisymmetric degeneracies are evaluated numerically for arbitrary initial disturbances expanded in terms of Chebyshev polynomials. The first symmetric and the first antisymmetric degeneracies exhibit temporal growth of the amplitudes in the wavenumber space. The maximum amplitudes are at most 7 times larger than the corresponding initial amplitudes. The amplitudes of the responses of the other four degeneracies decay rapidly owing to their higher damping rates. The time for which the degeneracy-response is in the growing phase is shown to be stretched with increasing Reynolds number. The degeneracies can therefore be active for longer periods of time at larger Reynolds numbers.

1. Introduction

The simplest approach to the question of laminar to turbulence transition in parallel shear flows is that by Orr & Sommerfeld (see e.g. Drazin & Reid 1981). For plane Poiseuille flow, the traditional two-dimensional investigations on the linear stability of the temporal Orr–Sommerfeld (OS) eigenmodes predict the critical Reynolds number R to be 5772.22 (Orszag 1971), where R is based on the centreline velocity and the channel half-height. Recent experiments on plane Poiseuille flow (Carlson, Widnall & Peters 1982; Alavyoon, Henningson & Alfredsson 1986) have shown that the initial stages of transition are accompanied by localized regions of turbulence known as turbulent spots. According to the latter, these spots cannot be generated for $R < 1100$, whichever the disturbance is, whereas for $R > 2200$, which is obviously an apparatus-dependent value, the turbulent spots appear randomly without the use of external excitation. The experimental transition R is hence much lower than the theoretical prediction for instability. Nevertheless, according to the above experiments, the turbulent spots are accompanied by strong oblique linear waves, suggesting the validity of the linear stability approach at least in some parts of the spot environment.

Extensive numerical computations of the Orr–Sommerfeld (OS) equation (Orszag 1971; Mack 1976) have shown that the major part of the temporal eigenmodes is stable, leading to exponential decay in time, and therefore, in general, considered

unimportant from the transition point of view. Detailed mappings of these stable eigenmodes, as carried out in this study, have revealed the interesting feature of degeneracy, i.e. two simple OS modes coalesce to form a single OS mode of order 2. Degeneracy can possibly lead to algebraic growth for a short initial period followed by eventual decay. This and other related features of importance, discussed in §2.2, are the main focuses of this study.

The earliest reference to degenerating eigenmodes seems to have appeared in the PhD thesis of Schensted (1961). Even though she did not consider this phenomenon to be probable in systems such as plane Poiseuille flow, she studied some of the mathematical consequences of degeneracy. Later, Betchov & Criminale (1966) came across a few pairs of coalescing eigenmodes, unexpectedly as claimed, in their calculations concerning combined stability problems, in space and time, of the inviscid laminar jet and wake. Gaster (1968) showed, by considering the analyticity of the characteristic function determining the eigenvalues, why eigenmodes of order 2 (i.e. degeneracies) *must* occur. He also analysed the influence of such modes on the perturbation generated by a pulse input. In the inviscid laminar jet and wake cases, the results seemed not in favour of the time-growing instability. Degeneracies among stable spatial OS eigenmodes in plane Poiseuille flow as well as in boundary-layer type mean flows were recently analysed by Koch (1986). He assessed the physical relevance of a degenerated mode pair by the inverse of the corresponding spatial damping rate. According to Koch, the spatial degeneracy mechanism plays a passive role in the laminar-to-turbulence transition in plane Poiseuille flow and an active role in boundary-layer type flows.

Degeneracies among stable temporal OS eigenmodes in plane Poiseuille flow are of concern in the present paper. A methodical search for these degenerating eigenmodes (§3) and their responses (§4) are the objectives of the study. The excitation of the degeneracies is studied through the initial-value problem, which seems well suited for the purpose, and the formulation of the problem follows somewhat that of Gustavsson (1986). The analyses are carried out in three-dimensional space, and thereby the obliquity of the linear waves is accounted for.

2. Analysis

2.1. *Problem formulation*

For plane Poiseuille flow, the evolution of the non-dimensionalized vertical component, $v(x, y, z, t)$, of a small three-dimensional perturbation velocity field is governed by the linearized equation

$$\left(\frac{\partial}{\partial t}+U\frac{\partial}{\partial x}\right)\nabla^2 v - U''\frac{\partial v}{\partial x} = \frac{1}{R}\nabla^4 v. \tag{1}$$

This equation has been rendered non-dimensional with channel half-height h and centreline velocity U_0 as the characteristic length and velocity scales. The Reynolds number is defined as $R = U_0 h/\nu$, where ν is the kinematic viscosity. x, y and z are the non-dimensional streamwise, vertical and spanwise directions, respectively. The dimensionless steady basic velocity profile is parabolic and is given by $U = 1-y^2$, and therefore $U'' = -2$, where the prime denotes the y-derivative. ∇^2 denotes the Laplacian. Solid walls, extending to infinity in the x- and z-directions, bound the flow at $y = \pm 1$. Thus the impermeable and no-slip conditions at the wall boundaries yield

$$v = \frac{\partial v}{\partial y} = 0 \quad \text{at} \quad y = \pm 1. \tag{2}$$

Double Fourier transformation of $v(x,y,z,t)$ on the homogeneous spatial coordinates x and z, with real positive wavenumbers α and β, respectively, and Laplace transformation on the time coordinate t, with complex s, transform (1) to

$$(\mathrm{D}^2-k^2)^2\phi-\mathrm{i}\alpha R\left(U+\frac{s}{\mathrm{i}\alpha}\right)(\mathrm{D}^2-k^2)\,\phi+\mathrm{i}\alpha RU''\phi=-R\Delta. \tag{3}$$

Here $\mathrm{D}=\mathrm{d}/\mathrm{d}y$, $k^2=\alpha^2+\beta^2$, and the forcing function Δ is given by

$$\Delta=\left(\frac{\partial^2}{\partial y^2}-k^2\right)\hat{v}\quad\text{at}\quad t=0, \tag{4}$$

where $\hat{v}=\hat{v}(\alpha,y,\beta,t)$ and $\phi=\phi(\alpha,y,\beta,s)$. By the transformation

$$s=-\mathrm{i}\alpha c, \tag{5a}$$

the homogeneous operator of (3) is identified with the traditional OS operator. Yet another transformation

$$c'=c+\mathrm{i}\frac{k^2}{\alpha R} \tag{5b}$$

is carried out in order to avoid the computational difficulties due to the presence of k^4 term in (3), at large values of k. Consequently (3) can be rewritten as

$$(\mathrm{D}^2-k^2)\,\mathrm{D}^2\phi-\mathrm{i}\alpha R(U-c')\,(\mathrm{D}^2-k^2)\,\phi+\mathrm{i}\alpha RU''\phi=-R\Delta, \tag{6a}$$

and the boundary condition (2) as

$$\phi=\mathrm{D}\phi=0\quad\text{at}\quad y=\pm1, \tag{6b}$$

where $\phi=\phi(\alpha,y,\beta,c')$.

The formal solution to (6a, b) obtained by the method of variation of parameters is given as (compare with Gustavsson 1986)

$$\phi=-R\left\{F_r+\frac{F_{13}}{E_{13}}+\frac{F_{24}}{E_{24}}\right\}, \tag{7a}$$

where

$$\begin{aligned}F_r(y)=\;&\phi_1(y)\left\{\int_0^y K_1(\eta)\,\Delta(\eta)\,\mathrm{d}\eta-\int_0^1 K_1(\eta)\,\Delta_{\mathrm{s}}(\eta)\,\mathrm{d}\eta\right\},\\&+\phi_3(y)\left\{\int_0^y K_3(\eta)\,\Delta(\eta)\,\mathrm{d}\eta-\int_0^1 K_3(\eta)\,\Delta_{\mathrm{s}}(\eta)\,\mathrm{d}\eta\right\}\\&+\phi_2(y)\left\{\int_0^y K_2(\eta)\,\Delta(\eta)\,\mathrm{d}\eta-\int_0^1 K_2(\eta)\,\Delta_{\mathrm{a}}(\eta)\,\mathrm{d}\eta\right\}\\&+\phi_4(y)\left\{\int_0^y K_4(\eta)\,\Delta(\eta)\,\mathrm{d}\eta-\int_0^1 K_4(\eta)\,\Delta_{\mathrm{a}}(\eta)\,\mathrm{d}\eta\right\},\end{aligned} \tag{7b}$$

$$\begin{aligned}F_{13}(y)=\;&-\phi_1(y)\int_0^1\{E_{23}K_2(\eta)+E_{43}K_4(\eta)\}\,\Delta_{\mathrm{s}}(\eta)\,\mathrm{d}\eta\\&-\phi_3(y)\int_0^1\{E_{12}K_2(\eta)+E_{14}K_4(\eta)\}\,\Delta_{\mathrm{s}}(\eta)\,\mathrm{d}\eta\end{aligned} \tag{7c}$$

and

$$\begin{aligned}F_{24}(y)=\;&-\phi_2(y)\int_0^1\{E_{14}K_1(\eta)+E_{34}K_3(\eta)\}\,\Delta_{\mathrm{a}}(\eta)\,\mathrm{d}\eta\\&-\phi_4(y)\int_0^1\{E_{21}K_1(\eta)+E_{23}K_3(\eta)\}\,\Delta_{\mathrm{a}}(\eta)\,\mathrm{d}\eta.\end{aligned} \tag{7d}$$

$\{\phi_\nu\}_{\nu=1}^4$ are the linearly independent solutions to the fourth-order linear homogeneous operator of (6a). (This operator will be referred to as the (reduced) OS operator.) $\{K_\nu\}_{\nu=1}^4$ are the cofactors of $\{\phi_\nu'''\}_{\nu=1}^4$, respectively, in the matrix

$$\tilde{\boldsymbol{W}}(y) = \begin{bmatrix} \phi_1 & \phi_2 & \phi_3 & \phi_4 \\ \phi_1' & \phi_2' & \phi_3' & \phi_4' \\ \phi_1'' & \phi_2'' & \phi_3'' & \phi_4'' \\ \phi_1''' & \phi_2''' & \phi_3''' & \phi_4''' \end{bmatrix}. \tag{8}$$

By successive differentiations of K_ν with respect to y, it can be shown that $\{K_\nu\}_{\nu=1}^4$ are the linearly independent solutions to the adjoint of the (reduced) OS operator and thus satisfy

$$(\mathrm{D}^2-k^2)\,\mathrm{D}^2K_\nu - \mathrm{i}\alpha R(U-c')(\mathrm{D}^2-k^2)K_\nu - 2\mathrm{i}\alpha RU'\mathrm{D}K_\nu = 0. \tag{9}$$

Since the (reduced) OS operator is symmetric in y, two of the four ϕ_ν, ϕ_1 and ϕ_3, are chosen to be symmetric and the other two, ϕ_2 and ϕ_4, antisymmetric with respect to $y = 0$. Therefore the functions ϕ_ν and their y-derivatives, at $y = 0$, are chosen such that

$$\tilde{\boldsymbol{W}}(y=0) = \text{Identity matrix}. \tag{10a}$$

The values of K_ν and their y-derivatives, at $y = 0$, are then calculated to be

$$\left.\begin{array}{cccccc} \nu = & 1 & 2 & 3 & 4 \\ K_\nu & 0 & 0 & 0 & 1 \\ K_\nu' & 0 & 0 & -1 & 0 \\ K_\nu'' & 0 & 1 & 0 & k^2+\mathrm{i}\alpha R(1-c') \\ K_\nu''' & -1 & 0 & -k^2-\mathrm{i}\alpha R(1-c') & 0 \end{array}\right\} \tag{10b}$$

The forcing function Δ can conveniently be split into symmetric and antisymmetric parts, Δ_s and Δ_a, as $\Delta = \Delta_\mathrm{s}+\Delta_\mathrm{a}$. Finally,

$$E_{mn} = \phi_m\phi_n' - \phi_m'\phi_n \quad \text{at} \quad y = 1 \quad (m,n = 1,2,3,4). \tag{11}$$

At a prescribed $k-\alpha R$ combination, the poles of ϕ in the c'-plane, see (7a), are the zeros of the characteristic function $E(c', k, \alpha R) = 0$, where

$$E = E_{13} = (\phi_1\phi_3' - \phi_1'\phi_3) = 0 \quad \text{at} \quad y = \pm 1 \tag{12a}$$

in the symmetric case, and

$$E = E_{24} = (\phi_2\phi_4' - \phi_2'\phi_4) = 0 \quad \text{at} \quad y = \pm 1 \tag{12b}$$

in the antisymmetric case.

Equations (12a,b) are the relations that determine the temporal (reduced) OS eigenvalues in the theory of normal modes. Thus a pole in the solution of the initial-value problem and an eigenvalue in the theory of normal modes refer to the same entity. The temporal eigenvalues (or the poles) c' of plane Poiseuille flow are purely discrete and infinite in number (Schensted 1961). With one exception, these eigenvalues lie in the fourth quadrant of the c'-plane up to about $\alpha R = 10000$, according to the numerical calculations of Orszag (1971) and Mack (1976). At some $k-\alpha R$ combinations, two of the simple eigenvalues degenerate into one, thus leading to an eigenvalue of order 2 (or a double pole). At these critical points, not only $E =$

0 but also $\partial E/\partial c' = 0$. Double poles occur in a systematic manner which is described in detail in §3. The consequences of the occurrences of the double poles are considered next.

2.2. *Response of a double pole*

For a prescribed $k-\alpha R$ combination and a specified forcing function Δ, the evaluation of the components of ϕ of (7a) is a matter of straightforward numerical computations. However ϕ, being in the Fourier–Laplace space, is not informative enough. Since the explicit time dependence is of major interest, $\hat{v}$ is recovered upon Laplace inversion of ϕ according to

$$\hat{v}(\alpha, y, \beta, t) = \frac{1}{2\pi \mathrm{i}} \int_{\gamma-\mathrm{i}\infty}^{\gamma+\mathrm{i}\infty} \phi(\alpha, y, \beta, s)\, \mathrm{e}^{st}\, \mathrm{d}s. \tag{13}$$

From the relations (5a, b),

$$s = -\alpha\left[\mathrm{i}c' + \frac{k^2}{\alpha R}\right].$$

Thus the integration in (13) is transformed to

$$\hat{v}(\alpha, y, \beta, t) = \frac{-\mathrm{i}\alpha}{2\pi \mathrm{i}} \int_{\infty+\mathrm{i}l}^{-\infty+\mathrm{i}l} \phi(\alpha, y, \beta, c') \exp\left[-\left(\mathrm{i}c' + \frac{k^2}{\alpha R}\right)\alpha t\right] \mathrm{d}c', \tag{14}$$

where $l = (\gamma/\alpha) + (k^2/\alpha R)$, and γ is so chosen that $c' = \mathrm{i}l$ lies above all the poles of ϕ.

The line integral of (14) can be transformed to a closed contour integral along contour Γ, which encloses all the poles of ϕ, provided the integrand in (14) integrated along Γ_r vanishes. Here Γ_r is a contour with infinite extensions, used for completing the contour Γ. Following the arguments of Schensted (1961), ϕ can be shown to be analytic everywhere except at its poles. Consequently, using the Residue theorem, the integration to be performed, after substituting ϕ of (7a), is the following:

$$\hat{v}(\alpha, y, \beta, t) = \frac{\mathrm{i}\alpha R}{2\pi \mathrm{i}} \sum_{j=1}^{\infty} \left\{ \int_{\Gamma_j} \left[\frac{F_{13}}{E_{13}} + \frac{F_{24}}{E_{24}}\right] \exp\left[-\left(\mathrm{i}c' + \frac{k^2}{\alpha R}\right)\alpha t\right] \mathrm{d}c' \right\}, \tag{15}$$

where the contour Γ_j, with infinitesimally small radius, encircles the isolated pole c_j' in the same sense as the contour Γ.

The contribution to $\hat{v}$ by an isolated pole $c_0'(= c_j')$ is then

$$\hat{v}|_{c_0'} = \frac{\mathrm{i}\alpha R}{2\pi \mathrm{i}} \int_{\Gamma_0} \frac{F}{E} \exp\left[-\left(\mathrm{i}c' + \frac{k^2}{\alpha R}\right)\alpha t\right] \mathrm{d}c', \tag{16}$$

where F and E represent F_{13} and E_{13} in the symmetric case, and F_{24} and E_{24} in the antisymmetric case.

If c_0' is a *simple pole*, by use of the Cauchy Integral formula, we obtain

$$\hat{v}|_{c_0'} = \mathrm{i}\alpha R \left[\frac{F}{\partial E/\partial c'}\right]_{c_0'} \exp\left[-\left(\mathrm{i}c_0' + \frac{k^2}{\alpha R}\right)\alpha t\right]. \tag{17}$$

when $c_{i0}' - (k^2/\alpha R) < 0$, $\hat{v}|_{c_0'}$ decays exponentially with time. Since all the poles considered in this study are of this type, the simple pole cases are of no interest.

If c_0' is a *double pole*, the Cauchy Integral formula yields

$$\hat{v}|_{c_0'} = \mathrm{i}\alpha R \frac{\partial}{\partial c'} \left\{ \frac{F}{E} (c' - c_0')^2 \exp\left[-\left(\mathrm{i}c' + \frac{k^2}{\alpha R}\right)\alpha t\right] \right\}_{c_0'}. \tag{18}$$

Considering the fact that both E and $\partial E/\partial c'$ vanish at the double pole and using Taylor series expansions of E and $\partial E/\partial c'$ about the double pole, (18) can be rewritten as

$$\hat{v}|_{c_0'} = \mathrm{i}\alpha R[r\,\mathrm{e}^{\mathrm{i}\theta}(\alpha t)+\rho\,\mathrm{e}^{\mathrm{i}\zeta}]\exp\left[-\left(\mathrm{i}c_0'+\frac{k^2}{\alpha R}\right)\alpha t\right], \tag{19a}$$

where

$$r\,\mathrm{e}^{\mathrm{i}\theta} = -\mathrm{i}\left[\frac{F}{G}\right]_{c_0'}, \qquad \rho\,\mathrm{e}^{\mathrm{i}\zeta} = \left[\frac{\partial F/\partial c'}{G}-\frac{FG_c}{G^2}\right]_{c_0'}, \tag{19b,c}$$

$$G = \frac{1}{2}\frac{\partial^2 E}{\partial c'^2}, \qquad G_c = \frac{1}{6}\frac{\partial^3 E}{\partial c'^3}. \tag{19d}$$

$\hat{v}|_{c_0'}$ is a function of y and αt. The time development of the amplitude R_r of $\hat{v}|_{c_0'}$ becomes

$$R_r = \alpha R[r^2(\alpha t)^2+2r\rho\cos(\theta-\zeta)(\alpha t)+\rho^2]^{\frac{1}{2}}\exp[c_{i0}(\alpha t)], \tag{20}$$

where $c_{i0} = c_{i0}'-(k^2/\alpha R)$ from (5b), and $c_{i0} < 0$ at the double poles investigated in this study.

It is seen from (20) that $R_r = \alpha R\rho$ at $\alpha t = 0$ and that R_r decays exponentially to zero as $\alpha t \to \infty$. The behaviour of R_r in the interval $\alpha t = 0$ to ∞ is crucially determined by the initial slope

$$\left.\frac{\partial R_r}{\partial(\alpha t)}\right|_{\alpha t=0} = \alpha R\rho\left[\frac{r}{\rho}\cos(\theta-\zeta)+c_{i0}\right]. \tag{21}$$

Three cases are of particular interest.

Case (a). When $(r/\rho)\cos(\theta-\zeta) > -c_{i0}$, the amplitude R_r grows with time for a short initial period and then decays to zero as shown in figure 1(a). The coordinate $(\alpha t, R_r)$ corresponding to the maximum point is given by

$$(\alpha t)_{\mathrm{m}} = \frac{-1}{c_{i0}}\left[\frac{1+\Omega}{2}\right]-\frac{\rho}{r}\cos(\theta-\zeta) \tag{22a}$$

and

$$(R_r)_{\mathrm{m}} = -\alpha R\frac{r}{c_{i0}}\left[\frac{1+\Omega}{2}\right]^{\frac{1}{2}}\exp[c_{i0}(\alpha t)_{\mathrm{m}}], \tag{22b}$$

where

$$\Omega = \left[1-4c_{i0}^2\frac{\rho^2}{r^2}\sin^2(\theta-\zeta)\right]^{\frac{1}{2}}. \tag{22c}$$

If $(R_r)_{\mathrm{m}}$ is large enough, the assumptions of the linear theory are violated and nonlinear effects may be initiated. The implications of such a state can only be analysed by nonlinear theories. On the other hand if $(R_r)_{\mathrm{m}}$ still lies within the range of the linear theory, the time taken for the maximum to be reached,

$$t_{\mathrm{m}} = \frac{(\alpha t)_{\mathrm{m}}}{\alpha R}R, \tag{23a}$$

plays an important role. Since αR is a given number for each double pole, increasing the Reynolds number stretches t_{m} so as to prolong the response of the double pole. Thus, the double pole acts almost as a neutrally stable mode, until $t = t_{\mathrm{m}}$, among the other exponentially decaying simple poles.

Case (b). When $(r/\rho)\cos(\theta-\zeta) \leqslant -c_{i0}$ and $\Omega^2 \leqslant 0$, R_r monotonically decays in time

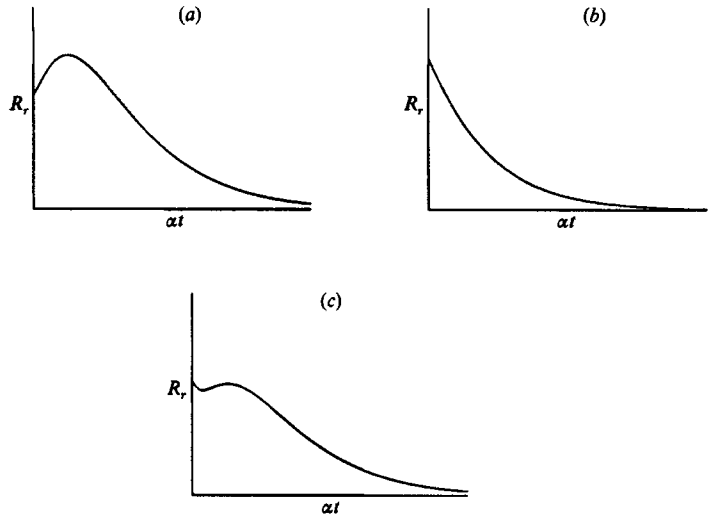

FIGURE 1. Temporal development of the amplitude R_r of the response $\hat{v}|_{c_0'}$ at a double pole. (*a*) Case (*a*); (*b*) case (*b*); (*c*) case (*c*).

as shown in figure 1 (*b*). Since the decay is not purely exponential, the rate at which R_r decays is characterized by the time taken for, say, 25% decay of the initial amplitude $\alpha R\rho$,

$$t_d = \frac{(\alpha t)_d}{\alpha R} R, \tag{23b}$$

where $(\alpha t)_d$ is the positive solution to the nonlinear equation

$$(0.75\rho)^2 = \{r^2(\alpha t)_d^2 + 2r\rho\cos(\theta-\zeta)(\alpha t)_d + \rho^2\}\exp\{2c_{i0}(\alpha t)_d\}. \tag{24}$$

The Reynolds number, in this case, stretches t_d so as to slow down the decay rate of R_r. This time-stretching effect, even though also present in the simple-pole cases, can be more pronounced in the double-pole cases since the decay of the double-pole response is not purely exponential at finite αt-values.

Case (*c*). When $(r/\rho)\cos(\theta-\zeta) \leqslant -c_{i0}$ and $\Omega^2 > 0$, an interesting possibility occurs. Under these conditions, the αt-values at which $\partial R_r/\partial(\alpha t) = 0$, are either both negative or both positive. Of these two cases, the former is equivalent to case (*b*) in the positive-αt range. In the latter, as αt increases from zero, R_r experiences two extrema, a minimum followed by a maximum, and then eventually decays to zero, as shown in figure 1 (*c*). The maximum point is expressed by $(\alpha t)_m$ and $(R_r)_m$ of (22*a*, *b*). Unlike in case (*a*), $(R_r)_m$ may or may not be larger than the initial amplitude $\alpha R\rho$. Consequently the time, which characterizes the temporal behaviour of R_r, is taken to be t_m of (23*a*) if $(R_r)_m \geqslant 0.75\alpha R\rho$ and to be t_d of (23*b*) if otherwise.

Apart from stretching the characteristic time, increasing R also increases β until $\beta = k$, as k and αR are constants at a double pole. In addition, since $\alpha \to 0$ as $R \to \infty$, structures elongated in the streamwise direction will be excited.

Which of the cases (*a–c*) will actually occur is discussed in §4.

3. The OS eigenmode structure and the degenerating pattern

3.1. *Numerical method*

Poles or (reduced) eigenvalues c' were evaluated, at prescribed k and αR, by numerically solving the (reduced) OS equation

$$(\mathrm{D}^2-k^2)\,\mathrm{D}^2\phi_\nu-\mathrm{i}\alpha R(U-c')\,(\mathrm{D}^2-k^2)\,\phi_\nu+\mathrm{i}\alpha RU''\phi_\nu=0, \tag{25}$$

with the condition that $\{\phi_\nu\}_{\nu=1}^4$ should satisfy the eigenvalue relation $E_{13}=0$ or $E_{24}=0$ at the wall $y=1$ (see (12*a*, *b*)). Adams interpolation formula with four steps was used for numerical integration of (25). Integration was started at the centreline $y=0$, with the values of ϕ_ν and their y-derivative specified by (10*a*), and proceeded towards the wall. Taylor expansion was used to evaluate the starting solutions at two backward points. The Gram–Schmidt orthogonalization procedure was used to eliminate the round-off error problem in cases where the growth of the solutions was so large as to destroy the eigenfunctions. Initially guessed values of c' were geared to convergence by the Secant method. This numerical scheme was adapted from that of Gustavsson (1981). The accuracy of the scheme was assured by comparing the calculated eigenvalues with those of Orszag (1971) and Mack (1976). Excellent agreement was observed with all but the unstable eigenvalue, which hardly converged. An increasing number of integration steps, between $y=0$ and $y=1$, were required for the convergence of c' as c_i' (the imaginary c') approached zero. In addition, convergence in this region demanded frequent orthogonalization steps when c_r' (the real c') was in the range of 0 to about $\frac{2}{3}$ and almost no orthogonalization when c_r' was in the range of about $\frac{2}{3}$ to unity.

3.2. *General behaviour of the eigenmodes*

The first set of eigenvalues were obtained at $k=0$ and at non-zero αR. This $k-\alpha R$ combination is physically absurd, but it served as a good starting point. Asymptotic expressions of the eigenvalue spectra at small αR-values, derived using regular perturbation expansions (see e.g. Drazin & Reid 1981, p. 158), at $k=0$ are

$$c'=\left(\frac{2}{3}-\frac{5}{2p_n^2}\right)-\mathrm{i}\left(\frac{p_n^2}{\alpha R}\right)\quad(n=0,2,4,\ldots),$$

with $p_n=(n+2)\,\pi/2$, in the symmetric case, and

$$c'=\left(\frac{2}{3}+\frac{5}{6q_n^2}\right)-\mathrm{i}\left(\frac{q_n^2}{\alpha R}\right)\quad(n=1,3,5,\ldots),$$

with $q_n\approx 1.430\pi,\ 2.459\pi,\ 3.471\pi,\ldots,\sim(n+2)\,\pi/2$ for larger n, in the antisymmetric case.

At $k=0$ and $\alpha R=25$, the eigenmodes are highly damped, and their streamwise phase velocities approach $\frac{2}{3}$ of the centreline velocity as the mode number increases. The eigenmodes have been numbered in the order of decreasing c_i' at a low αR-value. The locations of the symmetric (S) and the antisymmetric (A) eigenvalues in the c'-plane at $k=0$ and $\alpha R=5000$, traced by gradually increasing αR from about 25 to 5000, are shown in figures 2(*a*) and 2(*b*), respectively. As αR is increased from about 25 at $k=0$, the eigenvalues move in the direction of increasing c_i', the higher modes moving almost along the S-branch (line $c_\mathrm{r}'=\frac{2}{3}$), up to about $c_\mathrm{i}'=-0.35$. With further increase in αR, the eigenvalues move either towards $c'=(1,0)$, that is along the P-branch, or towards the origin $c'=(0,0)$. In the latter direction, the symmetric

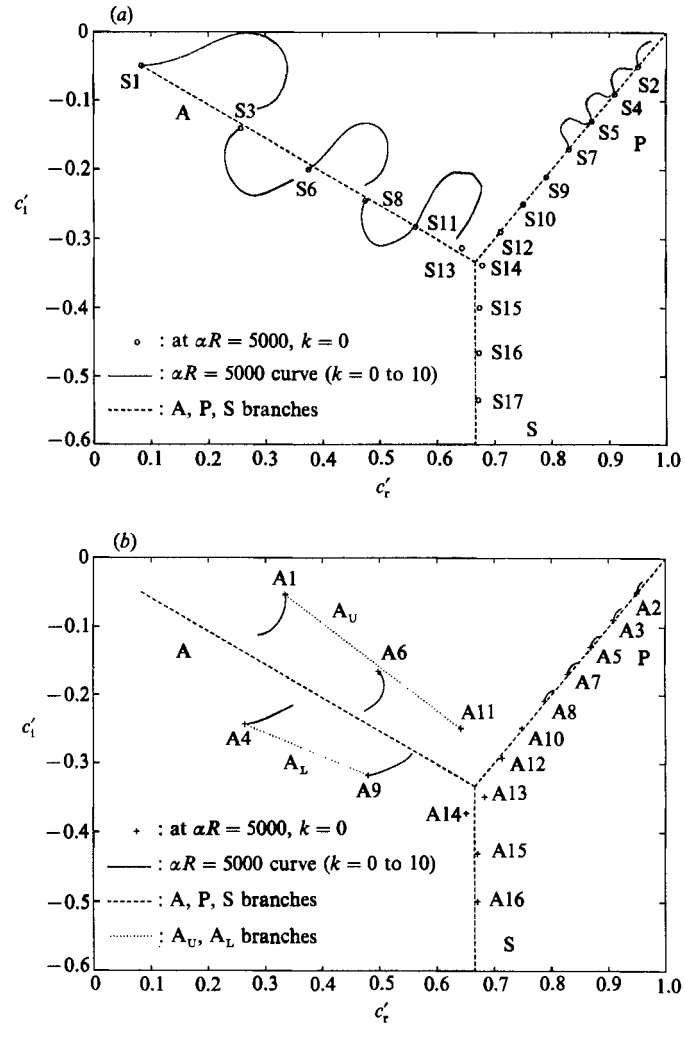

FIGURE 2. Locations of the least-damped OS (*a*) symmetric and (*b*) antisymmetric eigenmodes in the c'-plane, at $\alpha R = 5000$.

eigenvalues move along the A-branch whereas the antisymmetric eigenvalues move along the upper A-branch (A_U) or the lower A-branch (A_L). There exists a pattern in which the modes are distributed among the branches at increasing αR. This pattern, first found by Gustavsson (1986), is cyclic and has been confirmed in this study. The symmetric modes follow the order

$$A-P-A-P-P$$

for every 5-mode, and the antisymmetric modes follow the order

$$A_U-P-P-A_L-P$$

for every 5-mode. It is to be stressed here that even though the eigenmodes are grouped along three major branches A, P and S following the classification of Mack (1976), the grouping of this study has been carried out at $k = 0$, as in Gustavsson (1986), not at $k = 1$, as in Mack (1976).

As k increases from 0, the symmetric eigenvalues, which lie along the A-branch at $k = 0$ and at high αR ($= 5000$ in this case), move alternately to upper and lower sides of the A-branch, as shown in figure 2(*a*). With further increase in k, they curve back and move towards the A-branch. With increasing k, as shown in figure 2(*b*), the antisymmetric eigenvalues along the A_U and A_L branches at high αR ($= 5000$), also move towards the A-branch. Both the symmetric and antisymmetric eigenvalues along the P-branch at high αR curve back to the same branch in a simple manner, as k is increased. It is of relevance to realize that as $k \to \infty$, equation (25) approaches

$$D^2\phi_\nu - i\alpha R(U-c')\phi_\nu = 0.$$

This equation, with boundary conditions $\phi = 0$ at the wall $y = \pm 1$, yields the vertical vorticity eigenvalues which lie along the A, P and S branches. For more details about the vertical vorticity modes, the reader is referred to Gustavsson (1986).

In order to acquire a better insight into the behaviour of the eigenmodes, the first few of the symmetric as well as the antisymmetric eigenmodes are explored in detail in §§3.3 and 3.4.

3.3. *Symmetric modes*

Figure 3(*a*) shows how the eigenvalues corresponding to the first two symmetric modes S1 and S2 change their locations in the c'-plane with changing k and/or αR. Solid curves of figure 3(*a*) represent the $k = 0$ curves of both S1 and S2. The αR-curves of S1 are represented by the dashed curves and those of S2 by the dotted curves. (The curve along which k is a constant is referred to as the k-curve, and along which αR is a constant as the αR-curve.) The rings along each αR-curve represent $k = 2$, 3 and 10, respectively. When k increases from zero at constant αR, the higher αR ($= 500$ and 5000 for example)-curves of S1 curve back to the A-branch and those of S2 back to the P-branch, whereas the intermediate αR ($= 200$ and 100 for example)-curves extend across the c'-plane towards the opposite branch in either case. The αR-curves of both S1 and S2 not only characteristically change their shapes but also do so across the same range of αR. An enlarged view of this critical region, confined by the rectangle PQRS in figure 3(*a*), is given in figure 3(*b*) with a few more k-curves represented by solid lines. The $k = 2$ curve of S1 starting from $\alpha R = 200$ of S1 (point C) reaches $\alpha R = 500$ of S1 (point B), and then continue to move towards $c' = (0, 0)$ meeting the αR-curves of S1. The $k = 3$ curve of S1 starting from $\alpha R = 200$ of S1 (point D) reaches point E which lies on the $\alpha R = 500$ curve of S2 *not* of S1. With further increase in αR, this $k = 3$ curve moves towards $c' = (1, 0)$ meeting the αR-curves of S2, in contrast to the $k = 2$ curve of S1. Therefore one observes that the k-curves of S1 strikingly change their behaviour somewhere between $k = 2$ and $k = 3$ in the αR-range 200 to 500. Similar behaviour is also displayed by the k-curves of S2 as shown in figure 3(*b*), where points G, F, H and A are the counterparts of the points C, B, D and E, respectively.

The curious feature of figure 3(*b*) is what points A and E represent. Point A can represent either mode S1 at $k = 3$ and $\alpha R = 500$ or mode S2 at the same $k - \alpha R$ combination. The same is true for point E. These observations show that the modes S1 and S2, when put together, mutually complete each other. Consequently these modes lose or rather exchange their identities in the region enclosed by ABCDEFGHA in figure 3(*b*). The nature of this mode exchange suggests that it is connected with a mode coalescence, where two distinctly different eigenvalues degenerate into one single eigenvalue of order 2, i.e. to form a double pole. The k- and αR-ranges across which the eigenvalues degenerate are obviously the same ranges

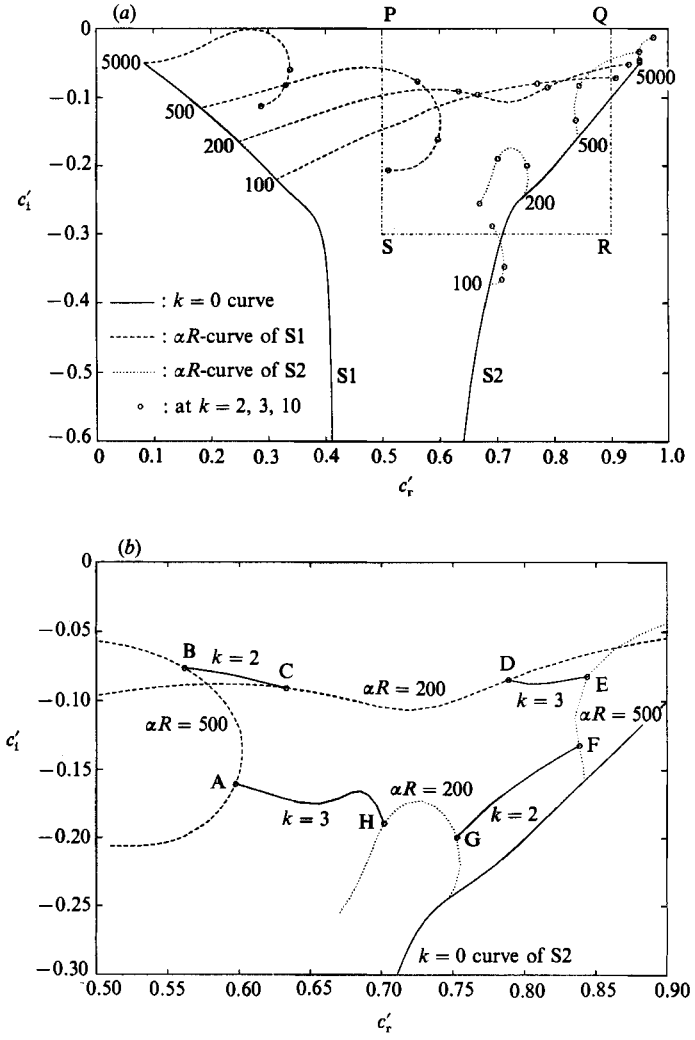

FIGURE 3. (*a*) Locations of the first two symmetric eigenmodes S1 and S2 in the c'-plane, and (*b*) a close look at the degenerating pattern, enlarged rectangle PQRS.

across which the k- and αR-curves significantly change their behaviour. Therefore the occurrence of a double pole and the k- and αR-ranges across which it occurs can easily be predicted by closely examining the detailed maps of the k- and αR-curves of the eigenmodes concerned.

Maps of the symmetric modes S3, S4 and S5 can be seen in figures 4(*a*), 4(*b*) and 4(*c*), respectively. The basic $k = 0$ curve and few αR-curves are shown. The maps of the first five symmetric modes S1 to S5 are different from each other; however, maps of the modes S6, S7, S8, S9 and S10, which are not produced in this paper, qualitatively resemble the maps of S1 to S5, respectively. This repetitive nature should not be surprising if one considers the cyclic nature in which the symmetric modes branch, as reported in §3.2.

The possible symmetric mode coalescences, obtained by carefully examining some of these maps, are reported in table 1. The degenerating mode pairs are joined by curves and the respective branches chosen by the modes at $k = 0$ are specified below

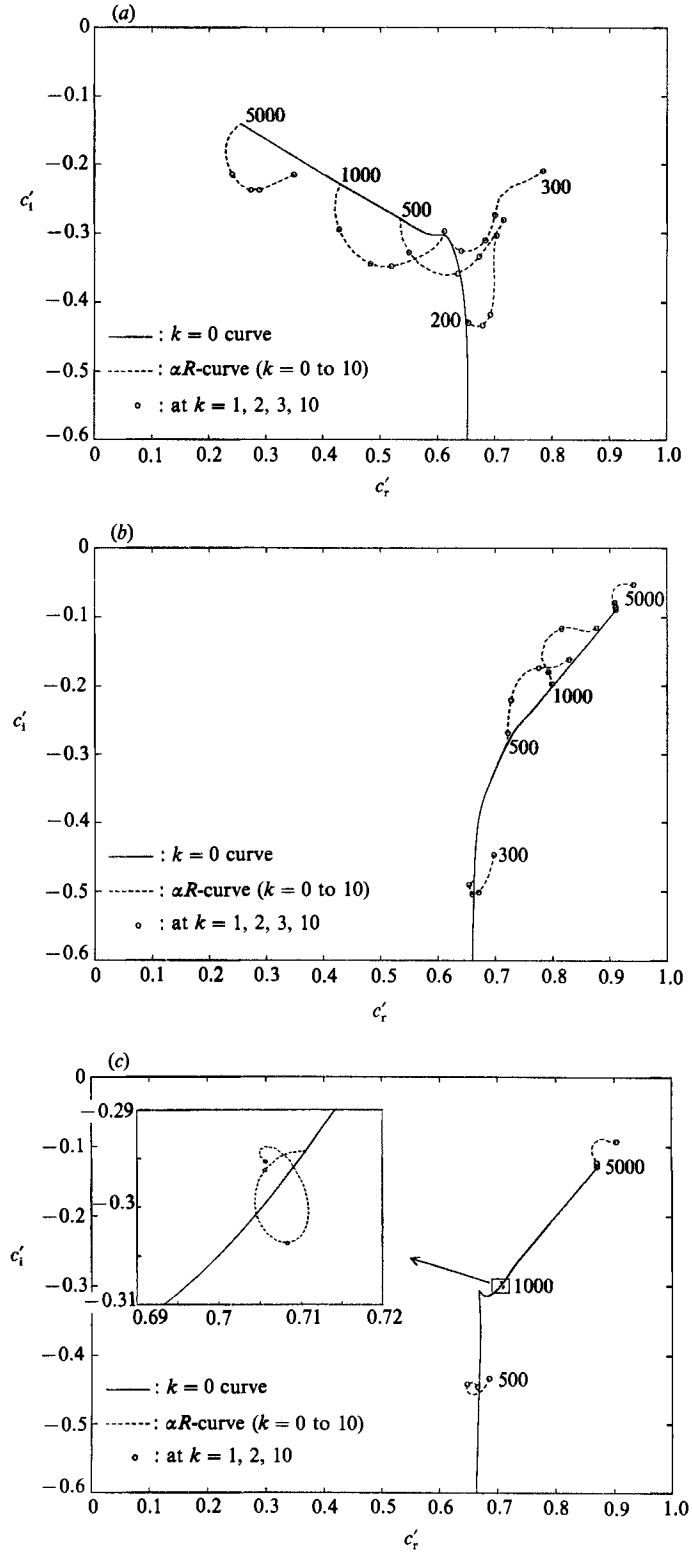

FIGURE 4. Locations of the symmetric modes (*a*) S3, (*b*) S4 and (*c*) S5 in the c'-plane.

Mode	S1	S2	S3	S4	S5	S6	S7	S8
Branch chosen at $k = 0$	A	P	A	P	P	A	P	A

TABLE 1. Degenerating symmetric mode pairs

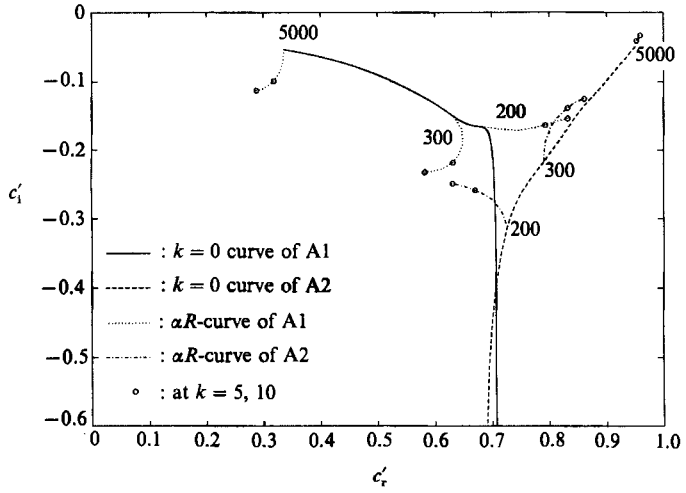

FIGURE 5. Degenerating pattern of the first two antisymmetric eigenmodes A1 and A2.

each mode. Table 1 provides a complete list of the degeneracies possible among the modes S1 to S7. The double curves between S5 and S6 reveal that it is possible for two modes to degenerate with each other more than once. Except for the bridging between modes S5 and S6, the pattern in which the modes degenerate seems to repeat for each 5-mode group, as indicated by table 1. The repetitive nature, already observed twice with the symmetric modes, strengthens the above speculation. Further discussion of the degeneracies follows a quick survey of the antisymmetric modes.

3.4. *Antisymmetric modes*

The first two antisymmetric eigenmodes A1 and A2 are shown in figure 5. The basic $k = 0$ curve and αR-curves at $\alpha R = 200$, 300 and 5000 of each mode are drawn. The characteristic changes in the shapes of αR-curves, shown in figure 5, and the associated k-curves behaviour are present with both A1 and A2. Consequently there is a degeneracy in the ranges $\alpha R = 200$–300 and $k = 0$–5.

Table 2 shows the degeneracies possible among modes A1 to A5. The fact that mode A3 does not degenerate at all can be explained by its map shown in figure 6, where the αR-curves of A3 more or less creep along the $k = 0$ curve. The k- and αR-curves of the antisymmetric modes, in general, span a smaller area of the c'-plane, as can be concluded from the maps of A1, A2 and A3 and the maps of A4 and A5, which are not produced here. This is probably why the number of degeneracies among the antisymmetric modes is comparatively smaller than the symmetric counterpart. In anticipation of a qualitative repetition of the maps as well as the degenerating pattern by each 5-mode group, no other antisymmetric modes were mapped.

Mode	A1	A2	A3	A4	A5
Branch chosen at $k = 0$	A_U	P	P	A_L	P

TABLE 2. Degenerating antisymmetric mode pairs

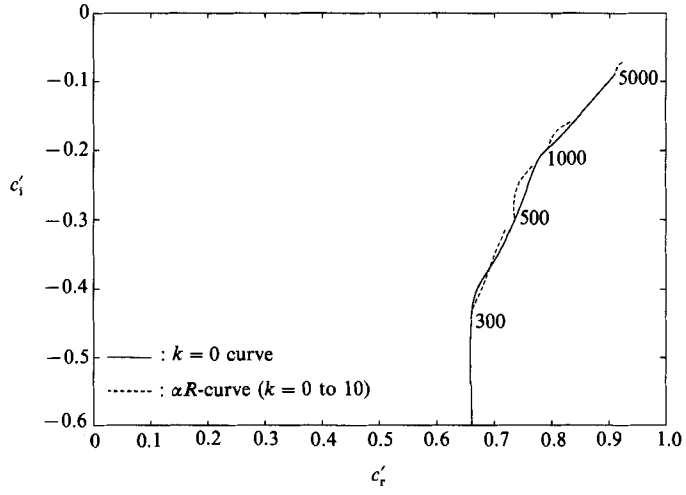

FIGURE 6. Location of the antisymmetric mode A3 in the c'-plane.

3.5. *Pin-pointing the double poles*

Having confined the first few degenerating mode pairs, we seek to pin-point the double poles with satisfactory accuracy. The poles c' are the zeros of the characteristic function $E(c', k, \alpha R)$, which is an entire function of c', k and αR. Its analytical properties can thus be exploited to obtain a dispersion relation in the vicinity of a double pole $(c_0', k_0, \alpha R_0)$. Both E and $\partial E/\partial c'$ are zero at a double pole so that a Taylor series expansion of E about such a point becomes

$$E(c', k, \alpha R) = (k-k_0)\left.\frac{\partial E}{\partial k}\right|_0 + (\alpha R-\alpha R_0)\left.\frac{\partial E}{\partial \alpha R}\right|_0 + (c'-c_0')^2\left.\frac{\partial^2 E}{2\partial c'^2}\right|_0$$
$$+ (k-k_0)(c'-c_0')\left.\frac{\partial^2 E}{\partial k\,\partial c'}\right|_0 + (\alpha R-\alpha R_0)(c'-c_0')\left.\frac{\partial^2 E}{\partial \alpha R\,\partial c'}\right|_0 + \ldots, \quad (26)$$

where $|_0$ represents the value at the double pole.

Since only the $(c', k, \alpha R)$ that are solutions to $E = 0$ are used in (26), $E(c', k, \alpha R)$ vanishes. Thus the dispersion relation obtained by the first approximation to (26) takes the following simple form:

$$(c'-c_0')^2 = A(k-k_0) + B(\alpha R-\alpha R_0), \quad (27)$$

where A and B are complex constants and can easily be deduced from (26).

The typical behaviour of the k- and αR-curves in the neighbourhood of a double pole is illustrated by figure 7, which displays the degenerating mode pair S1–S2. By knowing three points either along a constant αR-curve or along a constant k-curve, c_0' can readily be evaluated. With this c_0', and by exploiting the fact that the

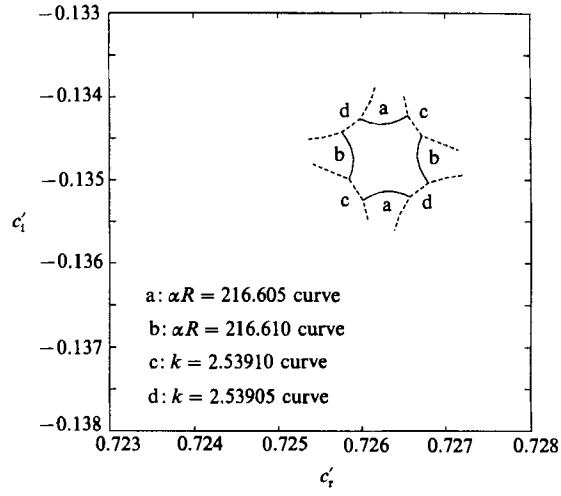

FIGURE 7. Behaviour of the degenerating modes S1 and S2 in the neighbourhood of the degeneracy S1–S2.

dispersion relation (27) is a mixture of real and complex entities, k_0 and αR_0 can easily be calculated. The reliance on these numerical values of c_0', k_0 and αR_0 to represent the double pole does of course increase as the curve concerned gets closer to the double pole. c_0' is then corrected by evaluating it from the eigenvalue relation $E = 0$, at the calculated k_0 and αR_0. The numerical zero of E is chosen to be $O(10^{-8})$. Since $\partial E/\partial c'$ also vanishes at the double pole, as a further check, $\partial E/\partial c'$ is numerically evaluated at the calculated c_0', k_0 and αR_0. Choosing a satisfactory numerical zero of $(\partial E/\partial c')|_{c_0'}$ can be achieved as follows. In the Taylor series expansion of E about the double pole, the terms $E|_{c_0'}$ and $(c'-c_0')(\partial E/\partial c')|_{c_0'}$ are dropped as they are identically zero. This step can numerically be justified when these terms are very small and of at least the same order. Since $E = O(10^{-8})$ and $(c'-c_0') \sim O(10^{-5})$, the numerical zero of $(\partial E/\partial c')|_{c_0'}$ can satisfactorily be chosen as $O(10^{-3})$. The dispersion calculations are repeated along curves closer and closer to the double pole until $(\partial E/\partial c')|_{c_0'}$ reaches the required order of magnitude. The $(c_0', k_0, \alpha R_0)$ at which it happens is taken to represent the double pole.

The major drawback in such a criterion to pin-point a double pole is the excessive number of eigenvalue computations required to pin-point one single double pole after it has been confined to coarse k- and αR-ranges. Dispersion relations obtained by higher approximations to the Taylor series expansion (26) seem to bring down the number of eigenvalue computations but, in reality, such relations led to either clumsy means or no means of pin-pointing c_0', k_0 and αR_0 and thus were discarded.

An elegant method of pin-pointing double zeros of a characteristic function has in fact been discussed by Gaster & Jordinson (1975). The function concerned was an analytical function of two complex variables, the streamwise wavenumber α and the frequency $\omega(=\alpha c)$. In the neighbourhood of the double zero, ω was expressed in terms of α as a sum of one regular series and the square-root of a second regular series. The rest of the calculations to pin-point the double zero was simple and rapid. An extension of such a method of series description to a more complicated problem, such as the one in this paper, is at the moment not clear. Nevertheless, an indirect and thus complicated way of employing the technique of Gaster & Jordinson to pin-point double zeros of a characteristic function in three variables has been discussed by

Mode pair	k_0	αR_0	c_0'	$R_{\min} = \alpha R_0/K_0$	abs $(\partial E/\partial c')_{c_0'}$
		Symmetric degeneracies			
S1–S2	2.539076	216.6076	0.7263537	85.3	0.0381
			−i0.1348152		
S3–S4	0.88582	363.7715	0.6406033	410.6	0.0018
			−i0.3499482		
S3–S5	1.891178	527.6455	0.6357061	279.0	0.0025
			−i0.3835066		
S5–S6	0.50635	904.2622	0.6691119	1785.8	0.0028
			−i0.3179580		
		Antisymmetric degeneracies			
A1–A2	2.2574	230.29	0.7193432	102.0	0.0031
			−i0.2073721		
A4–A5	2.8047	620.702	0.6444918	221.3	0.0002
			−i0.3969629		

TABLE 3. The first four symmetric and the first two antisymmetric degeneracies pin-pointed in this study, see also figure 8

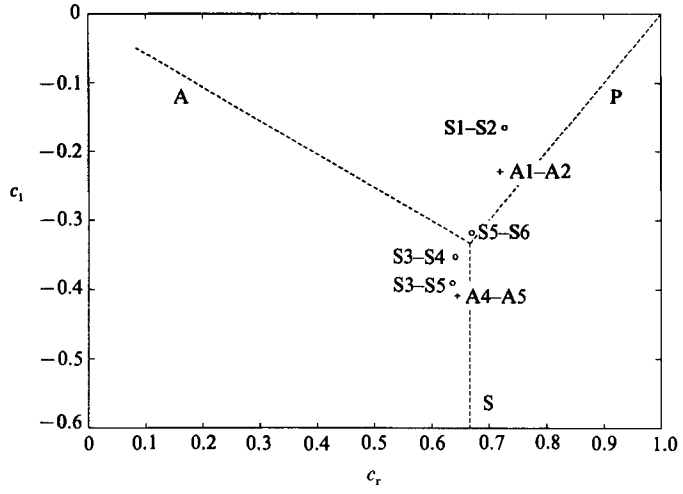

FIGURE 8. Locations of the first four symmetric (○) and the first two antisymmetric (+) degeneracies, listed in table 3, in the c-plane.

Koch (1986). However, we did not adapt Koch's procedure to our problem since Koch's method is not simpler than the method used in this work. A mathematically more elegant method of pin-pointing the double zeros of the characteristic function $E(c', k, \alpha R)$ is of interest since it will facilitate the analysis of more double poles of plane Poiseuille flow, and also the investigation of other flow systems, such as plane Couette flow.

The double poles pin-pointed in this study are listed in table 3 along with $R_{\min} = \alpha R/k$ and the absolute value of $(\partial E/\partial c')|_{c_0'}$. It seems, from tables 1 and 2, that one necessary condition for two modes to degenerate is that at $k = 0$, one of these two modes should choose the A-branch and the other the P-branch. It is in the neighbourhood of the point where the S-branch splits into A and P branches that the αR-curves change shape. Hence, the eigenmodes always degenerate in this region as typically demonstrated by figure 8, in which the degeneracies are shown in the c-

plane (not in the c'-plane). As a consequence, the degeneracies have streamwise phase velocities around $\frac{2}{3}U_0$ and damping rates in the range of 0 to about $-\frac{1}{2}U_0$. Considering the repetitive nature of the eigenmode behaviour, it is reasonable to assume that there is an uncountable number of double poles occurring in the above-described region, among the infinitely many isolated poles of plane Poiseuille flow. A formal mathematical proof of this conjecture should be possible but it was not attempted in this work.

4. Excitation of degeneracies

In this section, we discuss the quantitative measures of the responses of the first few degeneracies listed in table 3, when subjected to external excitations. The contribution to $\hat{v}$ by a double pole c_0', written as $\hat{v}|_{c_0'}$, was derived in §2.2 and is expressed by (19*a–d*). Evaluation of $\hat{v}|_{c_0'}$ requires knowledge of F ((7*c*) or (7*d*)), E ((12*a*) or (12*b*)), and their derivatives with respect to c', at the double pole. Evaluation of F and E requires that the linearly independent solutions, $\{\phi_\nu\}_{\nu=1}^4$ and $\{K_\nu\}_{\nu=1}^4$, of the OS equation (25) and its adjoint equation (9) be known. These equations were thus solved by numerical methods similar to that described in §3.1. In addition, the forcing function Δ_b, where $b = \mathrm{s}$ in the symmetric case, and $b = \mathrm{a}$ in the antisymmetric case, should be specified. Δ, given by (4), is determined by $\hat{v}(t = 0)$, the double Fourier-transformed vertical component of the *initial* perturbation velocity. For the sake of generality, the responses due to *any* but small disturbances are of interest. Therefore, $\hat{v}_b(t = 0)$ is taken to be arbitrary and thus can be expanded in terms of a complete set of orthogonal symmetric (or antisymmetric) functions. This also applies to Δ_b. As a first attempt, Δ is expanded in terms of the Chebyshev polynomials of the first kind $\{T_n\}_{n=0}^\infty$ as

$$\Delta_{\mathrm{s}}(y) = \sum_{n=0,2,4,\ldots} b_n T_n(y) \tag{28a}$$

and

$$\Delta_{\mathrm{a}}(y) = \sum_{n=1,3,5,\ldots} b_n T_n(y), \tag{28b}$$

where

$$T_n(y) = \cos(n \cos^{-1} y). \tag{28c}$$

The symmetric polynomials are given by even n and the antisymmetric by odd n.

The responses due to different members of the Chebyshev family were independently investigated. With n specified for T_n, the integration in (7*c*) or (7*d*) was numerically performed using Simpson's extended rule. The c'-derivatives of F and E at the double pole c_0' were evaluated by perturbing the functions concerned about c_0' by a small amount $\delta_{c'}$ and then by using appropriate finite-difference formulas. The reliability of the numerical value of the derivative in question has been affirmed by carrying out numerical experiments with different lengths of $\delta_{c'}$ and in different directions. The numerical values of $r\mathrm{e}^{\mathrm{i}\theta}$ (19*b*) and $\rho\mathrm{e}^{\mathrm{i}\zeta}$ (19*c*) changed very little when the number of numerical steps between $y = 0$ and $y = 1$ were increased from 300 to 600 through 60 steps at a time. The amplitude R_r of (20), evaluated at different y-positions with specified αt, remained unchanged when Δ_b given by T_n, which is purely real, was replaced by $T_n\mathrm{e}^{\mathrm{i}\lambda}$, where λ was varied from 0 to 2π.

The first symmetric double pole S1–S2, when excited by the polynomial T_4, exhibits temporal growth of the amplitude R_r in the sense of cases (*a*) and (*c*) described in §2.2. Growth is observed around the centreline of the channel ($y = 0$) and is shown in figure 9, at chosen y-positions. The largest ratio of the maximum

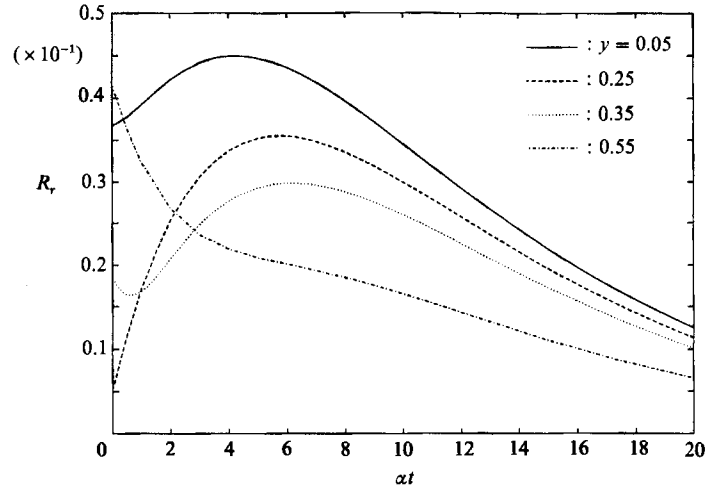

FIGURE 9. Temporal development of the amplitude R_r of the double pole S1–S2, at four different y-positions, when excited by T_4.

amplitude $(R_r)_m$ to the initial amplitude R_0 $(= \alpha R\rho)$, in this case, is about 6.605, occurring at $\alpha t = 5.743$, and is observed close to $y = 0.25$. However, the initial amplitude at $y = 0.05$, for instance, is greater than the maximum amplitude at $y = 0.25$, but the ratio of $(R_r)_m$ to R_0 at $y = 0.05$ is only 1.225. Thus, the chances of nonlinear consequences, initiated only by the magnitudes of $(R_r)_m$, seem slim in this case.

Nevertheless, the αt-values corresponding to $(R_r)_m$, at certain y-positions, suggest that the time-stretching phenomenon, discussed in §2.2, can be of importance. The (non-dimensional) time at which the maximum of R_r occurs at $y = 0.25$, for instance, is related to the Reynolds number, according to (23a), by

$$t_m = \frac{5.743}{216.6076} R = 0.0265R.$$

Despite of the smallness of the magnitude of (t_m/R), the characteristic time (t_m) spans the range 29.2 to 58.3 in the critical R range 1100–2200, discussed in the introduction. This means that the response of S1–S2, at $y = 0.25$, is in the growing phase until $t = 58.3$ at $R = 2200$, when excited by T_4. The numerical quantities above, however, should not be taken as final because T_4 alone is not Δ_s.

The first antisymmetric double pole A1–A2 also exhibits temporal growth in the sense of case (a), when excited by T_5. Growth is observed away from the centreline of the channel in contrast to that of S1–S2, and is shown in figure 10. The maximum amplitude at any y-position, in the case of A1–A2, does not exceed twice the corresponding initial amplitude.

The responses of S1–S2, when excited by the other symmetric Chebyshev polynomials, were also studied in detail and the results are demonstrated at a chosen y-position ($y = 0.25$) in figure 11. Growth in the sense of case (a) is observed with T_4 as discussed earlier. $T_4 = 8y^4 - 8y^2 + 1$, bounded by ± 1, has two zeros in the interval $y = [0, 1]$, and thus resembles a slightly distorted $\cos(2\pi y)$ function. Interestingly, the response of S1–S2 when excited by $\cos(2\pi y)$ is somewhat similar to the response due to T_4. The polynomials T_0 and T_2 give rise to higher initial

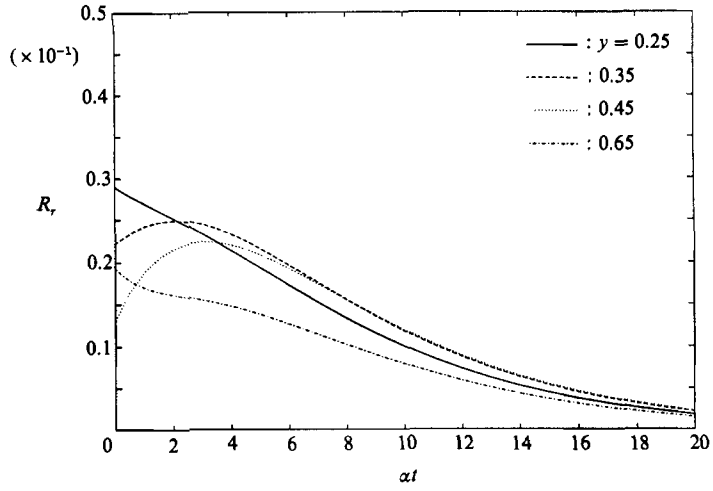

FIGURE 10. Temporal development of R_r of A1–A2, at four different y-positions, when excited by T_5.

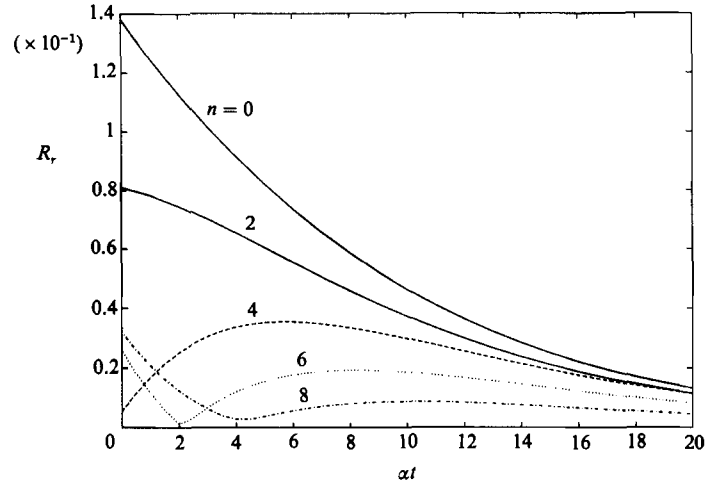

FIGURE 11. Temporal development of R_r of S1–S2, at $y = 0.25$, when excited by different T_n.

amplitudes than the other T_n do, but the amplitudes due to T_0 and T_2 monotonically decay to zero. In the interval $y = [0, 1]$, $T_0 = 1$ has no zero and $T_2 = 2y^2 - 1$ has one zero. When S1–S2 is excited by T_n ($n > 4$), growth in the sense of case (*a*) is seldom observed, but growth in the sense of case (*c*) is present. The time-stretching phenomenon is therefore in effect. As n increases, the number of zeros of T_n in $y = [0, 1]$ also increases, and the response of S1–S2 due to T_n becomes less and less pronounced as can be seen in figure 11.

The responses of A1–A2, when excited by the other antisymmetric Chebyshev polynomials are illustrated in figure 12 at a chosen y-position ($y = 0.35$). The polynomial $T_5 = 16y^5 - 20y^3 + 5y$, which causes growth in the sense of case (*a*), also has two zeros in $y = [0, 1]$. The qualitative behaviour of the responses of A1–A2 due to T_n ($n = 1, 3, 7, 9, \ldots$) resemble those of S1–S2 due to T_n ($n = 0, 2, 6, 8, \ldots$), respectively, and thus require no extra comments.

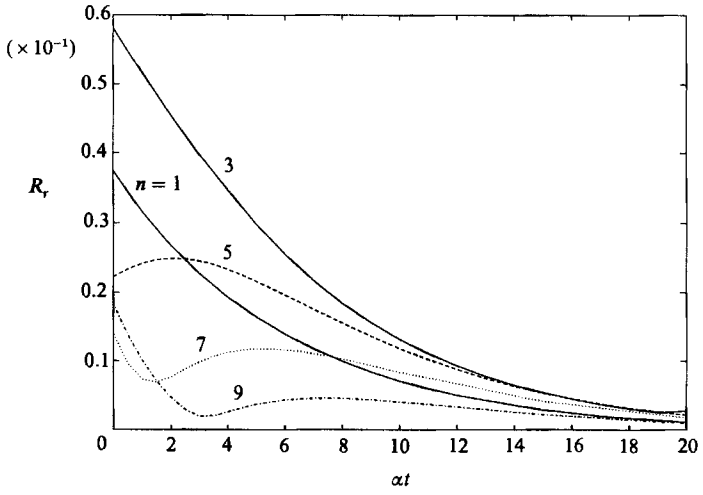

FIGURE 12. Temporal development of R_r of A1–A2, at $y = 0.35$, when excited by different T_n.

The overall response of a degeneracy due to the arbitrary forcing function Δ_b can, in principle, be evaluated by adding the responses due to different polynomials T_n, after weighting them by the corresponding constants b_n. The constants b_n can, though by a tedious means, be evaluated by substituting Δ_s and Δ_a, given by (28a, b), into

$$\int_0^1 \Delta_s(y) \cosh(ky)\, dy = 0 \tag{29a}$$

and

$$\int_0^1 \Delta_a(y) \sinh(ky)\, dy = 0, \tag{29b}$$

respectively. These conditions are deduced (see Gustavsson 1986) from the fact that $\hat{v_b}(t = 0)$ is subjected to the boundary conditions

$$\hat{v_b}(t = 0) = D\hat{v_b}(t = 0) = 0 \quad \text{at} \quad y = \pm 1. \tag{30}$$

The responses of degeneracies other than the first symmetric and the first antisymmetric ones, listed in table 3, were also investigated by exciting them by the Chebyshev polynomials. The temporal development of the amplitude R_r in each of these cases is rapid, though not purely exponential, decay to zero, as illustrated by figure 13(a, b). This behaviour is not surprising if one considers the corresponding damping rates c_{i0} ($= c'_{i0} - k^2/\alpha R$), given in figure 13(a, b), of these degeneracies. Therefore, it seems that the damping rate of a degeneracy could be used as an indicator in deciding whether or not that degeneracy be subjected to detailed analyses in search of growth and, hence, the consequences.

5. Discussion

Among the degeneracies listed in table 3, the first symmetric degeneracy S1–S2 and the first antisymmetric degeneracy A1–A2 exhibit temporal growth of the amplitudes. In the cases of the other four degeneracies, the amplitudes rapidly decay to zero. These results are, strictly speaking, valid only in the Fourier (wavenumber) space. But it is probable that the temporal histories of a degeneracy both in the Fourier space and in the real space are the same.

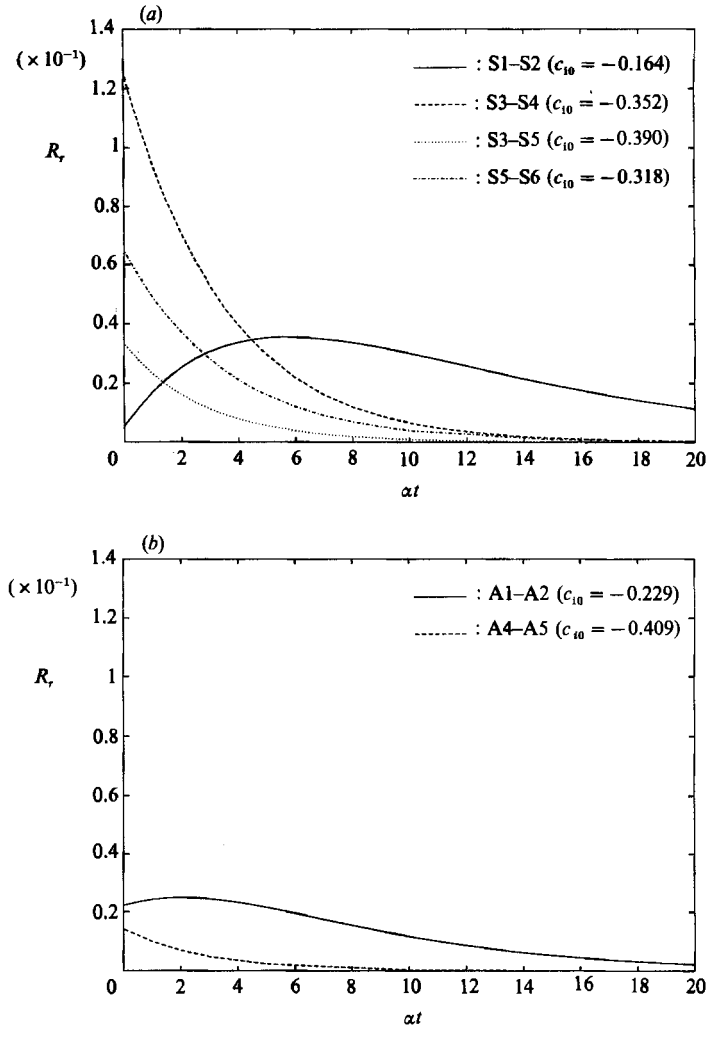

FIGURE 13. Temporal development of R_r corresponding to (*a*) the first four symmetric degeneracies, at $y = 0.25$, when excited by T_4, and (*b*) the first two antisymmetric degeneracies, at $y = 0.35$, when excited by T_5.

The damping rate of a degeneracy should, as a rule, be low enough for it to exhibit growth. In addition, $R_{\min}$ ($= \alpha R/k$) of a degeneracy should correspond to the laminar region for it to contribute to the transition mechanism. We have, however, analysed only six of the infinitely many degeneracies of plane Poiseuille flow. It seems, from table 3, that degeneracies among the higher eigenmodes may have higher damping rates and higher values of $R_{\min}$, and hence may be of marginal importance from the transition point of view, although we cannot prove that it is so.

The temporal (or spatial) responses of double poles rapidly developing into relatively large amplitudes, and their nonlinear consequences have also been the major concern of some past works, such as Benney & Gustavsson (1981), Koch (1986), Gustavsson (1986). None of these studies, including the present one, has so far given any *strong* evidence that the amplitudes of the double-pole responses can grow so large as to violate the assumptions of the linear theory.

However the time-stretching phenomenon discussed in this study, yet another facet of the degeneracy, can be active even if there is only a slight growth of the amplitude, as revealed by the degeneracy S1–S2 for instance. If the characteristic time, t_m of (23a), is stretched long enough, a new disturbance may see the basic profile not as parabolic but as parabolic plus the response of the degeneracy. Investigating the consequences of such a state is a natural development of the present study, and will be completed in due course. It seems that, among the degeneracies analysed in this study, S1–S2 and A1–A2 are the most suitable candidates to be subjected to further growth-related investigations.

We here digress to mention that strong linear waves, with wavenumber $k = 1.89$ and streamwise phase speed $c_r = 0.53$, accompanying turbulent spots in plane Poiseuille flow at $R = 1500$ were experimentally located by Henningson & Alfredsson (1987). The numerical simulations of a turbulent spot in plane Poiseuille flow, by Henningson (1988), also showed similar waves, having $k = 1.88$ and $c_r = 0.62$, at the same Reynolds number. Can these observations be accounted for by the degeneracy S3–S5, having $k = 1.891178$ and $c_r = 0.6357061$, despite the rapid decay of its response? A definite answer to this question awaits an enquiry into other possible aspects of degeneracies, such as their effects upon the disturbance energy.

I thank L. Håkan Gustavsson, my study supervisor, for suggesting the area of this research and for his continued interest. This work has in part been supported by the National Swedish Board for Technical Development through its program for basic research (STUF).

REFERENCES

Alavyoon, F., Henningson, D. S. & Alfredsson, P. H. 1986 Turbulent spots in plane Poiseuille flow – flow visualization. *Phys. Fluids* **29**, 1328–1331.

Benney, D. J. & Gustavsson, L. H. 1981 A new mechanism for linear and nonlinear hydrodynamic instability. *Stud. Appl. Maths* **64**, 185–209.

Betchov, R. & Criminale, W. O. 1966 Spatial stability of the inviscid jet and wake. *Phys. Fluids* **9**, 359–362.

Carlson, D. R., Widnall, S. E. & Peeters, M. F. 1982 A flow-visualization study of transition in plane Poiseuille flow. *J. Fluid Mech.* **121**, 487–505.

Drazin, P. G. & Reid, W. H. 1981 *Hydrodynamic Stability*, Chap. 4. Cambridge University Press.

Gaster, M. 1968 Growth of disturbances in both space and time. *Phys. Fluids* **11**, 723–727.

Gaster, M. & Jordinson, R. 1975 On the eigenvalues of the Orr–Sommerfeld equation. *J. Fluid Mech.* **72**, 121–133.

Gustavsson, L. H. 1981 Resonant growth of three-dimensional disturbances in plane Poiseuille flow. *J. Fluid Mech.* **112**, 253–264.

Gustavsson, L. H. 1986 Excitation of direct resonances in plane Poiseuille flow. *Stud. Appl. Maths* **75**, 227–248.

Henningson, D. S. 1988 Wave growth associated with turbulent spots in plane Poiseuille flow. *Rep.* FFA-TN-1988-08. Aero. Res. Inst., Bromma, Sweden.

Henningson, D. S. & Alfredsson, P. H. 1987 The wave structure of turbulent spots in plane Poiseuille flow. *J. Fluid Mech.* **178**, 405–421.

Koch, W. 1986 Direct resonances in Orr–Sommerfeld problems. *Acta Mech.* **58**, 11–29.

Mack, L. M. 1976 A numerical study of the temporal eigenvalue spectrum of the Blasius boundary layer. *J. Fluid Mech.* **73**, 497–520.

Orszag, S. A. 1971 Accurate solution of the Orr–Sommerfeld stability equation. *J. Fluid Mech.* **50**, 689–703.

Schensted, I. V. 1961 Contributions to the theory of hydrodynamic stability. PhD thesis, University of Michigan.